Semnan University

Mechanics of Advanced Composite Structures

journal homepage: http://MACS.journals.semnan.ac.ir

Electro-Elastic Analysis of Finite Length FGPM Cylinders Subjected to Electromechanical Loading Using First-Order Electric Potential Theory

M. Parhizkar Yaghoobi, M. Ghannad*

Faculty of Mechanical and Mechatronics Engineering, Shahrood University of Technology, Semnan, Iran

KEYWORDS

2D Electro-Elastic
FGPM Cylinders
Piezoelectric
Shear Deformation Theory
First-Order Electric Potential Theory

ABSTRACT

In this study, an analytical solution is presented based on the voltage feedback control method for the two-dimensional electro-elastic static response of functionally graded piezoelectric material (FGPM) cylinders. Using first-order shear deformation theory as well as first-order electric potential theory and applying the energy method, a differential equations system is extracted, which is solved as a classical eigenvalue problem. The results show the significant impact of heterogeneity on the electromechanical behavior of the cylinders. Furthermore, control gain affects the electric potential and electromechanical behavior of the head where the voltage is applied. The present research also introduces an analytical solution with no limitation to specific conditions in cylinder heads and without any need for convergence check. Moreover, the results show that any changes in cylinder head conditions affect the behavior of FGPM cylinders. The results were compared with those from the finite element method (FEM), leading us to a reasonable agreement.

1. Introduction

Nowadays, researchers are looking for materials that, in addition to being endowed with such features as constructional suitableness like low weight and high strength among others, would have other desirable properties with a view to a new revolution in structures, mechanical devices and equipment. Piezoelectric materials are substances in which electric fields are deformed or their deformation makes electric field in them. Piezoelectric materials can be considered as smart materials because the electromechanical behavior of these materials enables them to be used as sensors, actuators or active controllers of the structure. In order to improve the structures, the idea of functionally graded materials (FGMs) or heterogeneous materials was developed, which led to improved distribution properties changes. Such materials can prove to have better continuity and integrity properties than conventional composite materials, and their stresses and changes can have a continuous state which leads to an increase in the material strength. Therefore, researchers have focused on the behavior of structures with these materials by studying their behavior from different perspectives. Among the various structures, shells are of particular importance mainly due to the high efficiency of their behavior against load bearing. Many examples of these types of structures, such as dome roofs, tankers, fluid storage tanks, nuclear reactors, projectiles, missiles, etc., are found in artificial systems made by humans. These samples are also found in natural systems, for example, in skulls, shells and bones among others. These samples represent merely a limited portion of the extensive use of shells in natural and artificial systems [1, 2]. Among diverse shell geometries, cylinders have attracted researchers the most due to their high rate of usage and easy construction. That is why a section is dedicated to them in most curriculums and we review it in the relevant literature that follows.

Dai et al. in 2010 [3] obtained a heterogeneous electro-thermo-magneto-elastic analysis using the plane elasticity theory (PET). They considered the heterogeneity of the distribution of properties in the cylinder in an

* Corresponding author. Tel.: +98-23-32300240; Fax: +98-23-32300258
E-mail address: ghannad.mehdi@gmail.com; mghannadk@shahroodut.ac.ir

DOI: 10.22075/MACS.2020.19576.1236
Received 2020-01-15; Received in revised form 2020-05-06; Accepted 2020-06-19

exponential state. In their study, the heat transfer and electrostatic equilibrium were considered as one-dimensional and in radial direction. It was also assumed that the cylinder is in the uniform magnetic field located in the direction of its axis. That led to the creation of heterogeneous differential equations. By solving these equations and applying boundary conditions, they studied the electro-thermo-elastic behavior of the cylinder under electro-thermo-elastic loading. In the same year, Ghannad and Zamani-Nejad [4] analyzed the homogeneous double-headed clamped cylinder under internal pressure using First-Order Shear Deformation Theory (FSDT) and studied the shear stress in the cylinder. They showed that in areas far from the boundaries of the two cylinder's heads the shear stress tends to zero, causing stresses and displacements to be only a function of cylinder radius, while at the boundary it is a function of the radius and length of the cylinder. They also observed that at points far from the boundary, there is a good agreement between the theory of shear deformation and the plane elasticity. Ghorbanpour Arani et al. [5] presented an exact solution for an axisymmetric functionally graded piezoelectric (FGP) rotating disk with constant thickness subjected to an electric field and thermal gradient. Using PET, a nonhomogeneous second order differential equation is derived and solved.

In 2012, Ghannad and Zamani-Nejad [6], using the theory of plane elasticity and the definition of structural relationships in general state (plane stress and plane strain), obtained a complete solution to the heterogeneous thick wall cylinders that were under internal and external pressure. They considered the heterogeneity of properties for the elasticity modulus as the exponential state and assumed that the Poisson coefficient was constant. They also showed that in order to increase or decrease stress and displacement, positive or negative values should be taken for the heterogeneity constant. Also, they [7] analyzed the heterogeneous thick wall cylinders that were subjected to internal and external pressure, using the shear deformation theory.

In 2013, Dai and Jiang [8] investigated the electro-magneto-thermo-elastic behavior of a FGP solid cylinder. The solid cylinder was located in a uniform magnetic field and subjected to a thermal load, electric excitation, and pressure in the outer layer. Using long cylinder assumption (plane strain condition) and regardless of the end effects of the FGPM solid cylinder, they presented an analytical solution for the problem and studied the heterogeneity of properties effects on electro-magneto-thermo-elastic behavior. Kargarnovin et al. [9] presented the exact planar solution for electro-elastic analysis of FGP structures under thermo-electro-mechanical loadings. The material properties were assumed to vary exponentially along the thickness. Exploiting the potential functions for stress and induction, the solution was obtained in a closed form manner. The influence of material heterogeneity was examined against the electro-elastic reaction of the FGP media.

In 2014 and 2015, Ghannad and Gharooni [10-11], using the first-order shear deformation theory and higher-order, achieved the displacements field and stresses in the heterogeneous cylinder whose properties changed as an exponential function under internal and external pressure. Khorshidi and Bakhsheshy analyzed the Free Natural Frequency of an FG Composite Rectangular Plate Coupled with Fluid using Rayleigh–Ritz Method [12]. In this research, the influence of the main parameters of the problem on wet natural frequencies is discussed. Dynamic elasticity solution for a clamped, laminated cylindrical shell with two orthotropic layers bounded with a piezoelectric layer and subjected to impulse load distributed on inner surface was presented by Saviz [13].

Jabbari and Aghdam in 2015 [14] conducted the thermo-elastic analysis of three-layered cylinders, consisting of two piezoelectric homogeneous cylinders and a heterogeneous cylinder. Using PET, the governing differential equations of the problem at plane strain state and based on one-dimensional thermal hypothesis are solved. The impact of heterogeneity of properties and control of the mechanical behavior of the cylinder by piezoelectric layers was observed. A free vibration analysis of the FG rectangular nanoplates is investigated by Khorshidi et al. [15]. Nonlocal elasticity theory is employed and the effect of transverse shear deformation and rotary inertia is investigated by the exponential shear deformation theory. The effect of various parameters including nonlocal parameters and power law indexes on natural frequencies is studied.

Atrian et al., in 2015 [16] obtained a thermo-elastic analysis of piezoelectric heterogeneous cylinders that were axial-asymmetrically loaded. The electro-thermo-elastic behavior of the heterogeneous thick wall cylinder was investigated in two dimensions and in the radial and circumferential directions. The heterogeneity of the properties was modeled as an exponential function that was changed in the radial direction. In this study, the effect of heterogeneity and the effect of electro-thermo-elastic loading on heterogeneous cylinder behavior was investigated. The active forced vibration control of circular plates coupled with piezoelectric layers and laminated composite

rectangular plate resting on linear line support is presented by [17] and [18], respectively. The results of this research show that by applying control force at the plates, the amplitude of transverse deformation will be controlled and reduced.

Loghman and Parsa [19] using PET, extracted a closed form solution for the electro-magneto-thermo-elastic response to a thick double-layered cylinder made from a homogeneous interlayer and an FGPM outer layer. Ghannad and Parhizkar Yaghoobi in 2015 and 2017 presented the two-dimensional thermo-elasticity solution of homogeneous and heterogeneous thick wall cylinders that were placed under their thermomechanical loading on the inner and outer layers for different boundary conditions in two cylindrical heads [20-21]. Using the energy method and the first order shear deformation theory and assuming linear variations of the thermal field along the thickness, they obtained the system of governing equations. In their study, the effects of different boundary conditions on thermoelastic behavior of homogeneous and heterogeneous cylinders were studied. Arefi et al. [22] presented an analytical method for the three-dimensional free vibration analysis of an FG cylindrical shell integrated by two thin FGP layers. The FSDT and quadratic forms formulation are used for the displacement field and electric potential, respectively. Using the energy method and considering the von Karman nonlinear strain-displacement relations, the equations of motion are derived. In this research the effects of the non-homogeneity of materials and geometry on natural frequency are studied. The size-dependent free vibration analysis of a sandwich nanoplate is studied by Arefi and Zenkour [23]. In this paper, the governing equation are derived using FSDT and a cosine form for electric potential distributions. The influence of important parameters of the problem such as the applied electric, magnetic potentials, etc. on the vibration characteristics of the sandwich nanoplate are discussed.

The exact closed-form solution for sound radiation of vibrating circular plates coupled with piezo-electric layers is presented by [24]. In this paper, the effect of boundary conditions, piezo-electric thickness, and the piezoelectric layer on the acoustical parameters was examined and discussed in details. Using differential quadrature method (DQM), static analysis of FG solid circular and annular plates integrated with piezoelectric layers was performed by Alibeigloo [25]. It was assumed that the plate has various edge boundary conditions and whose material properties vary in an exponential law across the thickness. The effects of material heterogeneity, geometry parameter, and various boundary conditions on the response of FG structures were studied. Mehditabar et al. [26] conducted research on the thermos-elasticity analysis FGP rotating hollow cylindrical shell subjected to dynamic loads. The material properties were varied in radial direction of cylinder by a power function. Using DQM and finite difference methods, the solution of boundary/initial value equations of the problem are provided. Free vibrations of composite rectangular piezoelectric nanoplate using modified shear deformation theories are analyzed by Khorshidi et al. [27]. The governing equations are derived based on the energy method and using the exponential shear deformation and trigonometric shear deformation theories. The effect of small scale and geometry parameters on the natural frequency of composite rectangular piezoelectric nanoplate is studied.

Parhizkar Yaghoobi et al. [28] in 2018 performed a longitudinal piezoelectric heterogeneous cylinder (plane strain state) and thin piezoelectric heterogeneous discs (plane stress states) analysis of stress and active control analysis. In their research, they assumed that the internal surface of the structure is like a sensor and its external surface is like an actuator, and is based on the method of solving the Lame. They finally provided an exact one-dimensional solution (in radial direction). The effect of heterogeneity constant and control coefficient factor on the electro-thermomechanical behavior are studied. Arefi and Bidgoli [29] presented electro-elastic analysis of the piezoelectric doubly curved shells resting on Winkler's foundation subjected to applied voltage. Using the energy method and the first order shear deformation theory, they derived the system of governing equations. The influence of important parameters such as applied electric potential and Winkler's parameter were investigated on the electro-elastic behaviors of the structure.

Creep stress and strain in Laminated Composite Pressure Vessels are analyzed by Ghasemi and Hosseinpour [30]. The classical lamination theory is used to derive the governing equations as a second-order equation to determine the radial, circumferential, axial, and effective stresses in the cylinder wall. The effect of orientation of fibers on creep strain distribution in the wall of a cylinder is studied. The two-dimensional electro-elastic analysis of FG carbon nanotubes reinforced composite cylindrical pressure vessels integrated with piezoelectric face-sheets as sensor and actuator is extracted by Arefi et al. [31]. The governing equations of the problem are derived based on the principle of virtual work. Using the classical eigenvalue-eigenvector method the problem is solved and the electro-elastic behavior of the

structure is studied. Also, the effect of characteristics and distribution of porosity on the electro-elastic behavior of laminated vessels with piezoelectric face-sheets based on higher order modeling is analyzed by Arefi et al. [32].

The electro-elastic analysis of FG carbon nanotubes reinforced composite cylindrical shells with piezoelectric layers based on third-order shear deformation theory is done by Mohammadi et al. [33]. Using the classical method, the analytical solution for the problem is obtained and the results are discussed. The thermo-magneto-mechanical long-term creep behavior of three-phase nano-composite cylinder is investigated by Ghasemi and Hosseinpour [34]. The results show that the values of creep strain and radial displacement in the magnetic field are lower than without a magnetic field, for two lay-ups. Also, the effects of the magnetic field in the creep behavior of three-phase laminated composite cylindrical shells are analyzed by [35]. It was found that temperature increase in the magnetic field is less effective on the in-creased values of creep strain and radial displacement. The fluid-structure interaction of vibrating composite piezoelectric plates is investigated by Khorshidi and Karimi [36]. The governing equations are derived based on Hamilton's principle and using the exponential shear deformation theory and a cosine form for electric potential distributions. The natural frequencies of the fluid-structure system are computed using the Galerkin method and the influence of the main variables on natural frequencies are discussed.

Considering the literature background of the subject, it seems that the problem of two-dimensional solution of the electro-elasticity static response of FG thick wall cylinders in the general case of boundary conditions with a voltage feedback control method has not been taken into account, and electro-elastic analysis has been achieved only in limited cases with simplification in the boundary conditions. For this reason, using the first-order shear deformation theory, first-order electric potential theory and applying the energy method the governing equations to heterogeneous cylinders that are under electromechanical loading are obtained under arbitrary electromechanical boundary conditions with a voltage feedback control method. The governing equilibrium equations are arranged in the form of a set of ordinary differential equations, which are solved by analytical method. By applying arbitrary electromechanical boundary conditions with a voltage feedback control method in the two cylinder's heads, the analytical constants of ordinary differential equations system are obtained and the numerical results for the cylinder are shown under two different boundary conditions. These results are compared with the results of FEM.

2. Formulation and Derivation of Governing Equations

The analyzed cylindrical shell is axial symmetry in terms of geometry, properties, loading, and boundary conditions, and it is possible to neglect changes in the circumferential direction ($\frac{\partial}{\partial\theta}(\ )=0$); therefore, the functions representing the mechanical and electrical behavior are only a function of the radius r and the x axis of the cylinder.

According to what was stated, the displacement field in this case is as follows.

$$\begin{aligned} u_r &= u_r(r,x) \\ u_\theta &= 0 \\ u_x &= u_x(r,x) \end{aligned} \tag{1}$$

u_r, u_θ and u_x are the displacement components in radial, circumferential, and axial directions, and $u_r(r,x)$ and $u_x(r,x)$ are a function of cylinder radius and axis.

The studied cylindrical shell has a continuous wall and is made of heterogeneous and transversely isotropic materials, whose material property in the radial direction is different from the two other directions. The heterogeneity of properties in this research is considered as a power state similar to [7], and using the relationship (2) the heterogeneous modeling of properties for analysis is presented.

$$Pr(r) = Pr_i\left(\frac{r}{r_i}\right)^{n_{Pr}} = Pr_i\,\bar{r}^{\,n_{Pr}} \tag{2}$$

In the above relations r_i is the internal radius of the cylinder and Pr_i is the property of the material in the inner layer of the cylinder, which can have mechanical and electrical properties such as modulus of elasticity, density, Poisson ratio, piezoelectric constants and dielectric stability constants. n_{Pr} in Eq. (2) above is the heterogeneity constant for property; the heterogeneity constant can take positive and negative real values. It is noteworthy that $n_{Pr}=0$ denotes the homogeneous materials.

To use the first-order shear deformation theory, as shown in Fig. 1, the distance between each point of the cylindrical shell to its axis of symmetry *r* ranges is expressed as its distance to the midline of the cylinder *z* plus the distance from the middle layer to the cylinder *R* symmetry axis. This work causes the coordinate change the differential component from *r* to *z* (dr,(r,θ,x)→ dz,(r,θ,x)) [7].

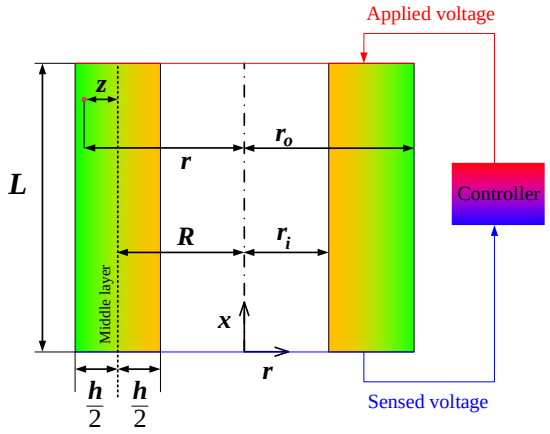

Fig. 1. Schematic of geometry and cross section of FGPM cylinder.

Given what has been said, we have.

$$r = R + z$$
$$R = \frac{r_o + r_i}{2} \tag{3}$$
$$h = r_o - r_i$$

Also, for z and x variations we have:

$$-\frac{h}{2} \le z \le \frac{h}{2}$$
$$0 \le x \le L \tag{4}$$

The displacement field for axial symmetric cylinder is described using the first order shear deformation theory as follows [7].

$$U_z = U_z(z,x) = U_z^0(x) + zU_z^1(x) = U_z^0 + zU_z^1$$
$$U_\theta = 0 \tag{5}$$
$$U_x = U_x(z,x) = U_x^0(x) + zU_x^1(x) = U_x^0 + zU_x^1$$

In the above relation, U_z, U_θ and U_x are the components of the displacement field along radial, circumferential and axial directions; also, according to the shear deformation theory, U_z^0 and U_z^1 have zero-order and one-order components of radial displacement, respectively and U_x^0 and U_x^1 are zero-order and one-order components of axial displacement, respectively which are only a function of axial coordination.

Also, using the first-order electric potential we have [37].

$$\varphi = \varphi(z,x) = \varphi^0(x) + z\varphi^1(x) = \varphi^0 + z\,\varphi^1 \tag{6}$$

Where φ^0 and φ^1 are respectively zero-order and first- order electric potentials, which are the only functions of the x-axis coordination.

The electric field and strain field are extracted using gradient relationships in the cylindrical coordinates [37] and the relations (5) and (6).

$$\varepsilon_z = U_z^1$$
$$\varepsilon_\theta = \frac{U_z^0 + zU_z^1}{R + z}$$
$$\varepsilon_x = \frac{\mathrm{d}U_x^0}{\mathrm{d}x} + z\frac{\mathrm{d}U_x^1}{\mathrm{d}x} \tag{7}$$
$$\gamma_{zx} = \frac{\mathrm{d}U_z^0}{\mathrm{d}x} + z\frac{\mathrm{d}U_z^1}{\mathrm{d}x} + U_x^1$$

ε_z, ε_θ and ε_x are radial, circumferential, and axial normal strains respectively. Also, γ_{zx} is the radial-axial shear strain.

$$E_z = -\varphi^1$$
$$E_\theta = 0 \tag{8}$$
$$E_x = -\frac{\mathrm{d}\varphi^0}{\mathrm{d}x} - z\frac{\mathrm{d}\varphi^1}{\mathrm{d}x}$$

E_z, E_θ and E_x are the components of the electric field in the radial, circumferential and axial directions respectively. The constitutive equations are expressed as follows [38].

$$\sigma_z = c_{11}\varepsilon_z + c_{12}\varepsilon_\theta + c_{12}\varepsilon_x - e_{11}E_z$$
$$\sigma_\theta = c_{12}\varepsilon_z + c_{22}\varepsilon_\theta + c_{23}\varepsilon_x - e_{12}E_z$$
$$\sigma_x = c_{12}\varepsilon_z + c_{23}\varepsilon_\theta + c_{22}\varepsilon_x - e_{12}E_z \tag{9}$$
$$\tau_{zx} = c_{55}\gamma_{zx} - e_{35}E_x$$
$$D_z = e_{11}\varepsilon_z + e_{12}\varepsilon_\theta + e_{12}\varepsilon_x + \in_{11}E_z$$
$$D_x = e_{35}\gamma_{zx} + \in_{22}E_x$$

In Eq. (9), σ_z, σ_θ, and σ_x are radial, circumferential and axial normal stresses respectively, τ_{zx} is the radial-axial shear stress, and D_z and D_x are the components of the electric displacement vector in radial direction and axial directions respectively. Also, c_{11}, c_{12}, c_{22}, c_{23}, and c55 are the elastic constants e_{11}, e_{12}, and e_{35} are piezoelectric-stress constants and $\in_{11}$ and $\in_{22}$ are the dielectric constants in the above-mentioned relationship.

For heterogeneity modeling in properties, the relationship (2) or power distribution is used, and the properties used in the structural relation (9) are modeled in an exponential state. So we will have.

$$c_{11} = c_{11i}\,\bar{r}^{\,n}; c_{12} = c_{12i}\,\bar{r}^{\,n}; c_{22} = c_{22i}\,\bar{r}^{\,n}; c_{23} = c_{23i}\,\bar{r}^{\,n}; c_{55} = c_{55i}\,\bar{r}^{\,n}$$
$$e_{11} = e_{11i}\,\bar{r}^{\,n}; e_{12} = e_{12i}\,\bar{r}^{\,n}; e_{35} = e_{35i}\,\bar{r}^{\,n}; \tag{10}$$
$$\in_{11} = \in_{11i}\,\bar{r}^{\,n}; \in_{22} = \in_{22i}\,\bar{r}^{\,n};$$

In the relation (10) c_{11i}, c_{12i}, c_{22i}, c_{23i}, and c_{55i} are the elastic constants values, e_{11i}, e_{12i}, e_{35i} are the piezoelectric-stress constants and $\in_{11i}$ and $\in_{22i}$ are the values of dielectric constants in the heterogeneous inner cylinder and n is the heterogeneity constant.

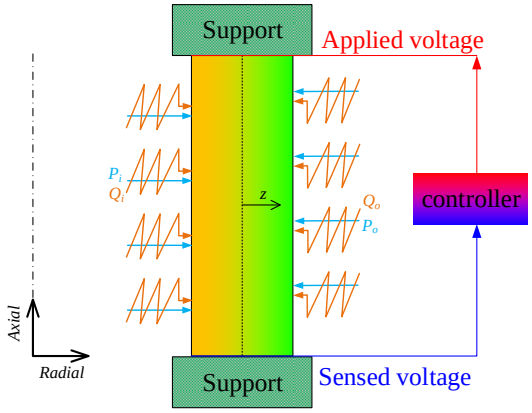

Fig. 2. FGPM cylinder cross section under loading on inner and outer surfaces.

Figure 2 shows the cross-section of a heterogeneous cylinder that is electromechanically loaded at its internal and external surfaces. As can be seen, the pressure P_i and the electric charge density Q_i are applied to the cylinder inner surface and the pressure P_o and the electric charge density Q_o are applied to the outer surface of the cylinder.

Mechanical and electrical resultants are defined as follows.

$$\begin{Bmatrix} N_z^m \\ N_\theta^m \\ N_x^m \end{Bmatrix} = \int_{-h/2}^{h/2} \begin{Bmatrix} \sigma_z\left(1+\frac{z}{R}\right) \\ \sigma_\theta \\ \sigma_x\left(1+\frac{z}{R}\right) \end{Bmatrix} \mathrm{d}z \tag{11}$$

$$\begin{Bmatrix} M_\theta^m \\ M_x^m \end{Bmatrix} = \int_{-h/2}^{h/2} \begin{Bmatrix} \sigma_\theta \\ \sigma_x\left(1+\frac{z}{R}\right) \end{Bmatrix} z\,\mathrm{d}z \tag{12}$$

$$\begin{Bmatrix} Q_x^m \\ M_{zx}^m \end{Bmatrix} = \int_{-h/2}^{h/2} \begin{Bmatrix} 1 \\ z \end{Bmatrix} \tau_{zx}\left(1+\frac{z}{R}\right)\mathrm{d}z \tag{13}$$

$$\begin{Bmatrix} N_z^e \bar{D}_z \\ N_x^e \bar{D}_x \end{Bmatrix} = \int_{-h/2}^{h/2} \begin{Bmatrix} D_z \\ D_x \end{Bmatrix} \left(1+\frac{z}{R}\right)\mathrm{d}z \tag{14}$$

$$M_x^e \bar{D}_x^1 = \int_{-h/2}^{h/2} D_x\left(1+\frac{z}{R}\right) z\,\mathrm{d}z \tag{15}$$

Based on the principle of virtual work, energy changes in the electromechanical potential of the structure are equal to the variation of work due to external forces applied to the structure $\delta w=\delta U$ [37, 39-40] where U is the total electromechanical energy of the whole body and W is the whole work due to the applied of the pressure and electrical charge density on the inner and outer surfaces of the cylinder. The energy of electromechanical potential of the whole body and the work resulting from these forces are calculated as follows.

$$\begin{cases} U = \iiint U^* \mathrm{d}\Omega;\ \mathrm{d}\Omega = r\mathrm{d}r\mathrm{d}\theta\mathrm{d}x = (R+z)\mathrm{d}z\mathrm{d}\theta\mathrm{d}x \\ U^* = \frac{1}{2}\left(\sigma_z\varepsilon_z + \sigma_\theta\varepsilon_\theta + \sigma_x\varepsilon_x + \tau_{zx}\gamma_{zx} - D_zE_z - D_xE_x\right) \end{cases} \tag{16}$$

$$W = \iint_S \left(P_i u_r\big|_{r=r_i} - P_o u_r\big|_{r=r_o} - Q_i\varphi\big|_{r=r_i} - Q_o\varphi\big|_{r=r_o}\right)\mathrm{d}S \tag{17}$$

In Eq. (17) the physical interpretation of the terms $-Q_i\varphi\big|_{r=r_i} - Q_o\varphi\big|_{r=r_o}$ are the electrical work done after applying the electrical surface charge density on the inner and outer surfaces of the cylinder respectively.

For work and energy changes, we have:

$$\begin{aligned} \delta U &= \int_0^L\int_0^{2\pi}\int_{-h/2}^{h/2} \left(\sigma_z\delta\varepsilon_z + \sigma_\theta\delta\varepsilon_\theta + \sigma_x\delta\varepsilon_x + \tau_{zx}\delta\gamma_{zx} - D_z\delta E_z - D_x\delta E_x\right)(R+z)\mathrm{d}z\mathrm{d}\theta\mathrm{d}x \\ \delta W &= \int_0^L\int_0^{2\pi}\left(\left(P_i\delta u_r\big|_{r=r_i} - Q_i\delta\varphi\big|_{r=r_i}\right)\left(R-\frac{h}{2}\right) - \left(P_o\delta u_r\big|_{r=r_o} + Q_o\delta\varphi\big|_{r=r_o}\right)\left(R+\frac{h}{2}\right)\right)\mathrm{d}\theta\mathrm{d}x \end{aligned} \tag{18}$$

By substituting the Eqs. (7-9) in (18), the application of the principle of virtual work and performing mathematical operations and simplifying, the system of governing equations is obtained as follows.

$$\begin{cases} 1 \to \delta U_x^0 \to R\frac{\mathrm{d}N_x^m}{\mathrm{d}x} = 0 \\ 2 \to \delta U_x^1 \to R\left(Q_x^m - \frac{\mathrm{d}M_x^m}{\mathrm{d}x}\right) = 0 \\ 3 \to \delta U_z^0 \to R\left(\frac{N_\theta^m}{R} - \frac{\mathrm{d}Q_x^m}{\mathrm{d}x}\right) = P_i\left(R-\frac{h}{2}\right) - P_o\left(R+\frac{h}{2}\right) \\ 4 \to \delta U_z^1 \to R\left(\frac{M_\theta^m}{R} + N_z^m - \frac{\mathrm{d}M_{xz}^m}{\mathrm{d}x}\right) = \frac{h}{2}\left(P_i\left(\frac{h}{2}-R\right) - P_o\left(R+\frac{h}{2}\right)\right) \\ 5 \to \delta\varphi^0 \to R\frac{\mathrm{d}\bar{D}_x}{\mathrm{d}x} = Q_i\left(R-\frac{h}{2}\right) + Q_o\left(R+\frac{h}{2}\right) \\ 6 \to \delta\varphi^1 \to R\left(\bar{D}_z - \frac{\mathrm{d}\bar{D}_x^1}{\mathrm{d}x}\right) = \frac{h}{2}\left(Q_i\left(R-\frac{h}{2}\right) - Q_o\left(R+\frac{h}{2}\right)\right) \end{cases} \tag{19}$$

Also, for boundary conditions we have:

$$\left[N_x^m\delta U_x^0 + M_x^m\delta U_x^1 + Q_x^m\delta U_z^0 + M_{zx}^m\delta U_z^1 + \bar{D}_x\delta\varphi^0 + \bar{D}_x^1\delta\varphi^1\right]\Big|_{0,L} = 0 \tag{20}$$

3. Analytical Solution of FGM Piezoelectric Cylinders

In this section an analytical solution for the equation system (19) is presented. As shown in the system of Equations (19), mechanical and electrical resultants are more numerous than the equations. Therefore, it is not possible to solve the system of equations (19) on the basis of resultants, and the equations (19) must be expressed on the basis of displacement field (4 unknown components) and electric potential (2 unknown components) so that they would be solved. Thus, using the relations (11) to (15) (definition of mechanical and electrical resultants) and the relations (5) to (10) and applying mathematical operations, the governing equations system is rewritten as equations (21) based on the displacement field and electric potential components. So we will have:

$$\begin{cases} \tilde{A}\frac{\mathrm{d}^2}{\mathrm{d}x^2}\vec{y} + \tilde{B}\frac{\mathrm{d}}{\mathrm{d}x}\vec{y} + \tilde{C}\frac{\mathrm{d}^2}{\mathrm{d}x^2}\vec{y} = \vec{F} \\ \vec{y} = \left\{U_z^0 \quad U_z^1 \quad \frac{\mathrm{d}U_x^0}{\mathrm{d}x} \quad U_x^1 \quad \frac{\mathrm{d}\varphi^0}{\mathrm{d}x} \quad \varphi^1\right\}^T \\ \vec{F} = \left\{K_9 \quad 0 \quad F_3 \quad F_4 \quad F_5x + K_{10} \quad F_6\right\}^T \end{cases} \tag{21}$$

Where $\tilde{A}_{6\times6}$, $\tilde{B}_{6\times6}$, and $\tilde{C}_{6\times6}$ are the coefficients matrices and $\vec{F}_{6\times1}$ and $\vec{y}_{6\times1}$ are respectively electromechanical force quasi-vector and electromechanical quasi-vector, whose non-zero components are defined and presented in Appendix A. Moreover, the "T" superscript shows the transpose of quasi-vector. K_9 and K_{10} are solved constants created by integrating the first and fifth equations of governing Eq. (19), and F_3 to F_6 are presented in Appendix A. Solving this equation's system consists of two parts; particular solving section $\vec{y}_p$ and general solving section $\vec{y}_g$.

$$\vec{y} = \vec{y}_g + \vec{y}_p \tag{22}$$

3.1. Particular Solution

As can be seen from Eq. (21), the heterogeneous part of the differential equation system is a first-order polynomial. Therefore, solving a particular part is considered as a first-order polynomial with non-definite coefficients. Therefore, we have:

$$\vec{y} = \vec{y}_{p1} x + \vec{y}_{p0} \tag{23}$$

These indefinite (unknown) coefficients become definite (known) as follows.

$$\begin{aligned} \vec{y}_{p1} &= \tilde{C}^{-1} \times \{0 \quad 0 \quad 0 \quad 0 \quad F_5 \quad 0\}^T \\ \vec{y}_{p0} &= \tilde{C}^{-1} \times \left(\{K_9 \quad 0 \quad F_3 \quad F_4 \quad K_{10} \quad F_6\}^T - \tilde{B} \vec{y}_{p1} \right) \end{aligned} \tag{24}$$

3.2. General Solution

To solve the general problem, the equation system should be solved in the following form.

$$\tilde{A} \frac{\mathrm{d}^2}{\mathrm{d}x^2} \vec{y} + \tilde{B} \frac{\mathrm{d}}{\mathrm{d}x} \vec{y} + \tilde{C} \frac{\mathrm{d}^2}{\mathrm{d}x^2} \vec{y} = \vec{0} \tag{25}$$

The general solution is considered in the following form.

$$\vec{y}_g = \vec{\varsigma} \mathrm{e}^{mx} \tag{26}$$

The general solution form of (26) is valid for Equation (21) when the coefficients matrix C does not have zero rows or columns. For this purpose, in deriving equations (21), the first and fifth equations of the system of equations (19) have been integrated. Furthermore, in defining the electromechanical quasi-vector, instead of zero-order axial displacement component and zero-order component of electric potential, their derivatives have been used.

By substituting the relation 26 in equation 25, the eigenvalue problem is obtained.

$$\left(\tilde{A} m^2 + \tilde{B} m + \tilde{C} \right) \vec{\varsigma} \mathrm{e}^{mx} = \vec{0} \tag{27}$$

To this end, the determinant of the Eq. (27) must be set to zero.

$$\det\left(\tilde{A} m^2 + \tilde{B} m + \tilde{C} \right) = 0 \tag{28}$$

By solving the above eigenvalue problem whose eigenvalue equation is an eight-order one and by finding eigenvalue vectors, the following general solution is obtained.

$$\vec{y}_g = \sum_{i=1}^{8} K_i \vec{\varsigma} \mathrm{e}^{m_i x} \tag{29}$$

Therefore, the solution of the system of equations (21) is obtained.

$$\left\{ U_z^0 \quad U_z^1 \quad \frac{\mathrm{d}U_x^0}{\mathrm{d}x} \quad U_x^1 \quad \frac{\mathrm{d}\varphi^0}{\mathrm{d}x} \quad \varphi^1 \right\}^T = \sum_{i=1}^{8} K_i \vec{\varsigma} \mathrm{e}^{m_i x} + \vec{y}_p \tag{30}$$

Given that (30) yields the obtained solution for the derivatives of the functions U_x^0 and φ^0, in order to obtain these functions, it is necessary to integrate the proposed solution for the derivation of these functions, in which case the constants K_{11} and K_{12} are obtained. Now these boundary constants are obtained by applying boundary conditions in the two cylinder heads.

3.3. Boundary Conditions

In this section, an adaptive voltage feedback control method is applied to supply control voltage for activating the voltage in the upper cylinder head. It is assumed that the voltage of lower cylinder head ($\varphi_L = \varphi(z,0)$) that is without electrical surface charge is measured by the embedded voltage sensor and fed back to the upper cylinder head as a control voltage by the controller. The control voltage used for operating the upper cylinder head is proportional to the voltage of lower cylinder head with a control gain (control factor) C_f and may be expressed as follows [14, 28, 41].

$$x = 0 \rightarrow \begin{Bmatrix} N_x^e \\ M_x^e \end{Bmatrix} = \begin{Bmatrix} 0 \\ 0 \end{Bmatrix}; \; x = L \rightarrow \begin{Bmatrix} \varphi^0(L) \\ \varphi^1(L) \end{Bmatrix} = C_f \begin{Bmatrix} \varphi^0(0) \\ \varphi^1(0) \end{Bmatrix} \tag{31}$$

The mechanical boundary conditions in both cylinder's heads could be of essential conditions. For example, the equation for the cylinder with two clamped heads in these conditions is as follows:

$$x = 0, L \rightarrow \begin{Bmatrix} U_z^0 \\ U_z^1 \\ U_x^0 \\ U_x^1 \end{Bmatrix} = \begin{Bmatrix} 0 \\ 0 \\ 0 \\ 0 \end{Bmatrix} \tag{32}$$

The mechanical boundary conditions on the two cylindrical heads can be a combination of essential and natural conditions, for example, for a cylinder with lower clamped head and upper free head, the mechanical boundary conditions in both heads of the cylinders are expressed as follows:

$$x = 0 \rightarrow \begin{Bmatrix} U_z^0 \\ U_z^1 \\ U_x^0 \\ U_x^1 \end{Bmatrix} = \begin{Bmatrix} 0 \\ 0 \\ 0 \\ 0 \end{Bmatrix}; \; x = 0 \rightarrow \begin{Bmatrix} N_x^m \\ M_x^m \\ Q_x^m \\ M_{zx}^m \end{Bmatrix} = \begin{Bmatrix} 0 \\ 0 \\ 0 \\ 0 \end{Bmatrix} \tag{33}$$

Therefore, by applying the boundary conditions on the two cylindrical heads – 6 conditions in one head (4 mechanical conditions and 2 electrical conditions) and 6 conditions on the other head (4 mechanical conditions and 2 electrical conditions) – K_1-K_{12} constants can be

achieved. It is noteworthy that the process of mathematical solution using coding in MAPLE 13 software is achieved.

4. Results and Discussion

For a numerical study, a heterogeneous cylinder with an inner and outer diameter of 40 mm and 60 mm respectively and a length of 800 mm is considered. The internal layer of this heterogeneous cylinder is made of PZT-4 and has the mechanical and electrical properties mentioned in the inner layer in accordance with Table 1 [42].

In order to study the effect of heterogeneity of properties and control gain on the electromechanical behavior of the cylinder, the heterogeneity constant (n) for the values n = 2, 1, 0, -1 and -2, and the control gain (C_f) for the values C_f = -10, -5, 0, 5, 10 and 10, are studied. It is noteworthy that the inner layer of this cylinder under the surface charge density is $15\times10^{-7}\,(\mathrm{C/m^2})$ and its outer layer is under pressure of 6 bar. This heterogeneous cylinder is studied in two cases: (a) two clamped heads; and (b) one lower clamped head and the upper free head. The static electric field that causes depolarization (E_{de}) often varies between $2\times10^5\,(\mathrm{V/m})$ and $5\times10^5\,(\mathrm{V/m})$, depending on the temperature of the applied electrical field [43]. The maximum amount of electric field imposed by C_f = 10 inside the cylinder is about $1.5\times10^5\,(\mathrm{V/m})$ that it is less than the lower limit of the assumed depolarizing electric field. The select ranges for the control factor must be chosen based on the amount of electrical surface charge density at the inner and outer surfaces of the cylinder.

In order to validate the results, the voltage of the lower end of cylinder (b) was assumed at zero. Figs. 3 and 4 show the distribution of radial displacement and electric potential in the FG cylinder (b) for validation. The results are predicted based on two analytical methods (present research and PET [28]) and FEM.

Table 1. Mechanical and electrical properties of the inner layer of FGPM cylinder.

Properties of PZT-4		
Elastic constants (GPa)	c_{11}	115
	c_{12}	74
	c_{22}	139
	c_{23}	78
	c_{55}	25.6
Piezoelectric-stress constants ($\mathrm{C/m^2}$)	e_{11}	15.6
	e_{12}	-5.2
	e_{35}	12.7
Dielectric Constants ($10^{-8}\mathrm{C/Vm}$)	ϵ_{11}	0.562
	ϵ_{22}	0.646

Figure 5 shows the distribution of electric potential, radial and axial displacement in FG cylinders. Because of the existence of electrical and mechanical boundary conditions at the two ends of the cylinder and the interaction of these conditions caused by the piezoelectricity of the cylinder, the distribution field of the displacement field and the electric potential near the boundaries are non-uniform.

Furthermore, in cylinder (a) or a cylinder with two clamped heads, where electrical boundary conditions in two cylinder heads (Eq. (31)) are non-uniform, the contour of the radial displacement behavior distribution is not symmetric with respect to the middle of the cylinder length; It is rather slightly asymmetric.

As can be seen in Fig. 5, cylinder (b), unlike cylinder (a), has only one mechanical constrained head and the upper head is free; this causes the maximum amount of displacements values to increase substantially in the cylinder. The greatest increase is related to the axial displacement of the cylinder, where the amount of maximum axial displacement has increased about 40 times. The radial and axial displacement changes along the thickness (except for axial displacement near the boundaries) are negligible, but the electric potential along the thickness has considerable variation.

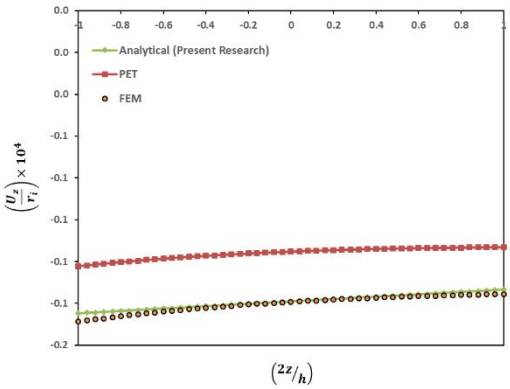

Fig. 3. Distribution of radial displacement in the middle length of FGP cylinder (n=1).

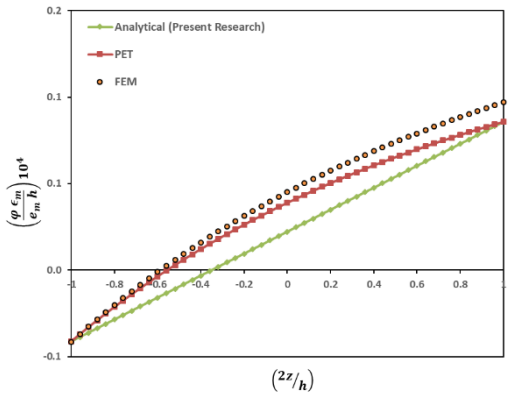

Fig. 4. Distribution of electric potential in the middle length of FGP cylinder (n =1).

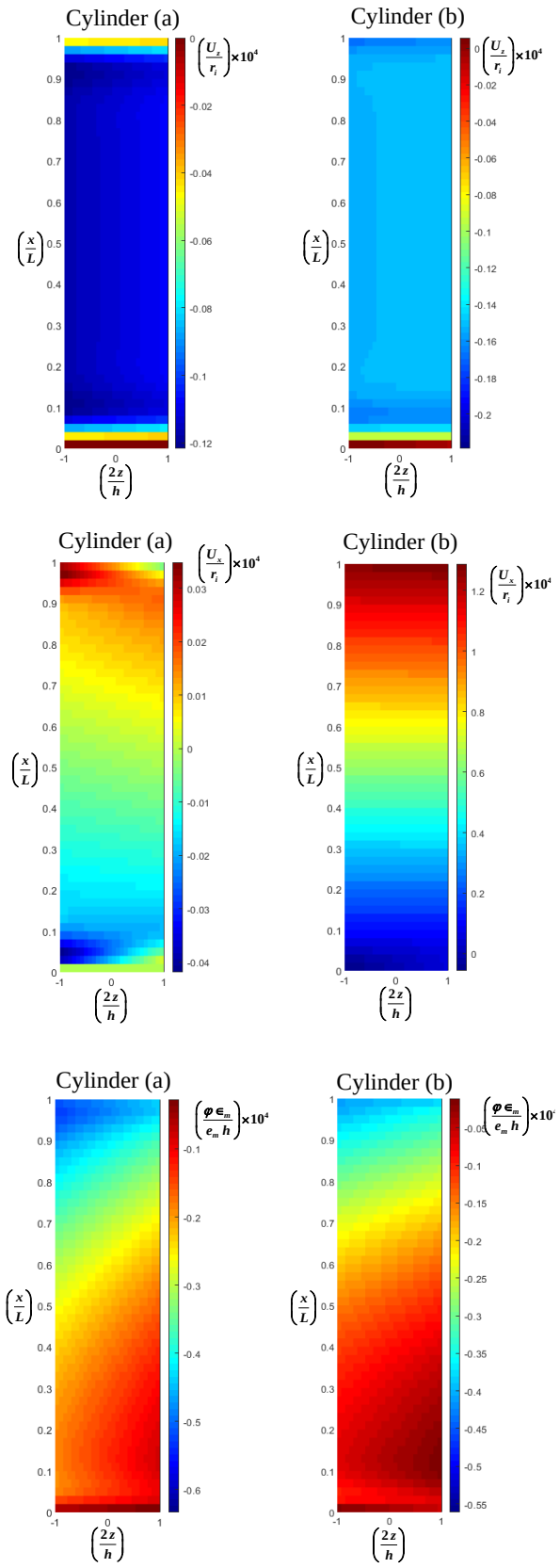

Fig. 5. Distribution of radial and axial displacement and electric potential in FG cylinders (n=2, C_f =10).

In fact, the electric potential sensitivity to the cylinder's thickness is greater than the sensitivity of the displacement field to the thickness. Maximum displacement values occur in or near the boundary areas (cylinder's head). Therefore, when considering the requirements of the design, engineers should pay attention to the boundary areas of the structure.

Figures 6 and 7 show the radial and axial displacement distribution in the inner and middle layer of heterogeneous cylinders respectively. Reduction of heterogeneity causes a significant increase in the distribution of displacement values. But it has no effect on the location of the emergence of maximum displacement values, and the maximum displacement values occur in the border regions or near the boundaries. As can be seen, the non-constrained state of one cylinder head causes the maximum displacement to increase, which is a larger increase in axial displacement and is more significant.

Although in the initial review it seems that Fig. 7 is not true for cylinder (b), by considering the mechanical conditions related to the two ends of the cylinder (b) compared with cylinder (a), the axial displacement behavior in the longitudinal direction is valid. Cylinder (a) is a clamped-clamped ends one while cylinder (b) is a clamped-free ends one. As can be seen in Fig. 5, a little away from the lower end of the cylinder (clamped condition), the supportive effects of the lower boundary on the axial displacement behavior vanishes and the axial displacement along the longitudinal distribution is almost linear.

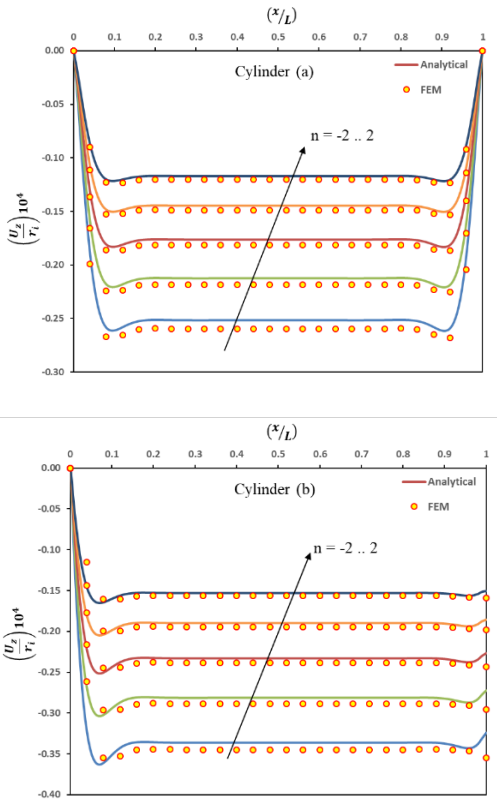

Fig. 6. Distribution of radial displacement in the inner layers of FG cylinders (C_f =0).

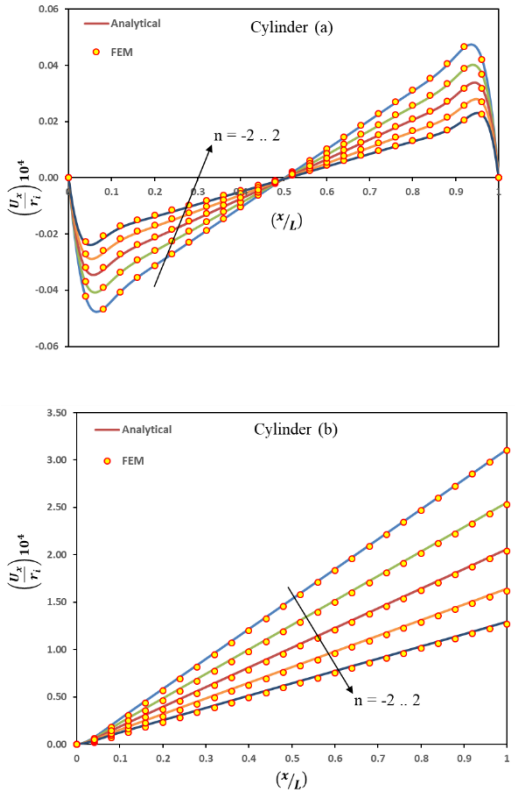

Fig. 7. Distribution of axial displacement in the middle layer of FG cylinders (C_f =0).

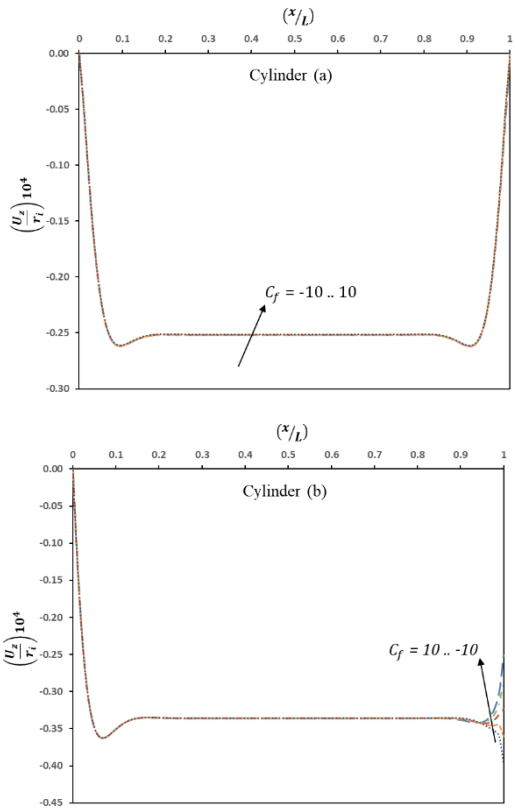

Fig. 8. Result of control gain on radial displacement in the inner layer of FG cylinders (n = -2).

Figures 8 and 9 show the effect of control gain on the radial and axial displacement in the inner and middle layer of heterogeneous cylinders respectively. Generally, the effect of control gain on the radial and axial displacement can be ignored and it doesn't cause a remarkable effect on radial and axial displacement; however, this effect is more visible in the heads of cylinder where the control voltage is applied.

Figure 10 shows the distribution of electric potential in the outer layer of the heterogeneous cylinder (em and ϵm are the average of piezoelectric-stress and dielectric constants in the inner layer of FG cylinder respectively). An increase in the heterogeneity constant causes the distribution of the electric potential in the heterogeneous cylinder decrease; in other words, the increase in heterogeneity constant leads to a decrease in the intensity of electric potential changes in the heterogeneous cylinder. The maximum and minimum values of electric potential occurred near the cylinder heads (boundary areas). Therefore, designers and engineers should pay attention to this issue when using and designing piezoelectric heterogeneous cylinders.

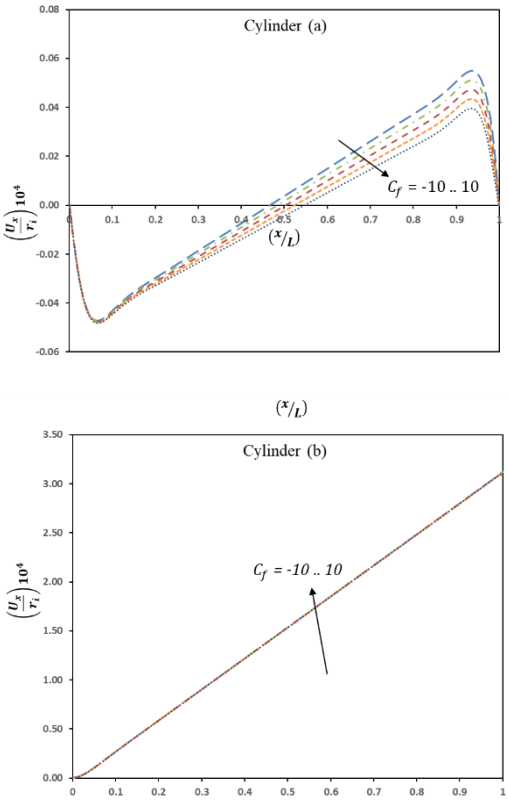

Fig. 9. Result of control gain on axial displacement in the middle layer of FG cylinders (n = -2).

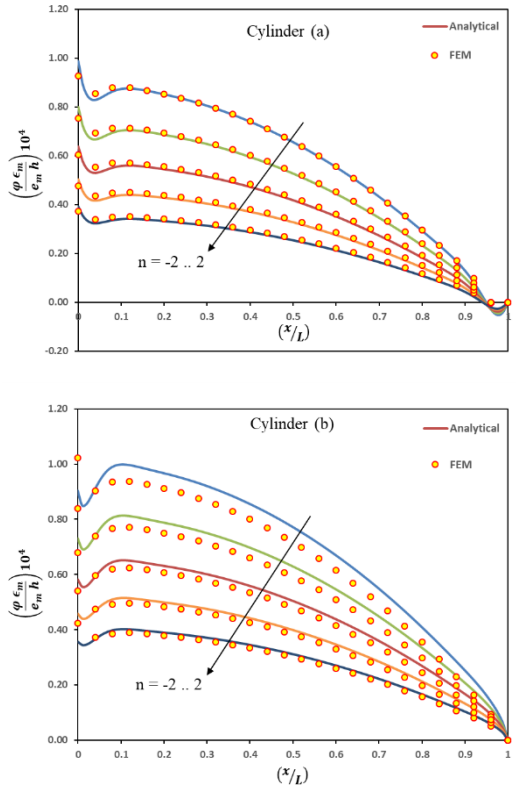

Fig. 10. Distribution of electric potential in the outer layer of FGPM cylinders (C_f=0).

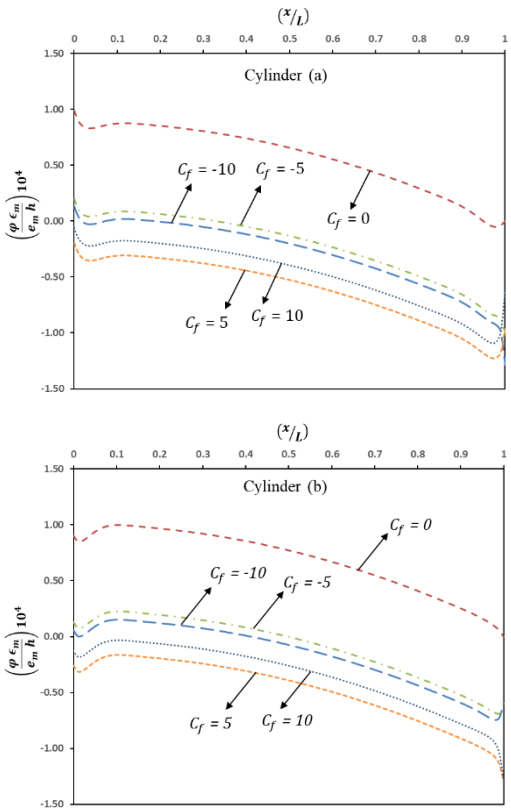

Fig. 11. Result of control gain on electric potential in the outer layer of FG cylinders (n = -2).

Figure 11 shows the effect of control gain on the electric potential in the outer layers of FG cylinders. The control gain has significant effects on the electric potential behavior profile especially in the upper head of cylinder where the voltage is applied. In order to better consider and evaluate the control gain effect on electric potential in the middle of the middle layer, the ζ is defined based on Eq. (33),which $\varphi(0,L/2)$ and $\varphi^{1.25}(0,L/2)$ are the electric potential in the middle of the middle layer with arbitrary control gain value and C_f=1.25, respectively.

Figure 12 illustrates the effect of control gain on electric potential behavior of FG cylinders in z=0 and x=$L/2$. Fig. 10 predicts the same behavior for control-ability FG cylinder structure like [35] by highlighting the effect of cylinder heads or cylinder boundary conditions. It shows changes in the boundary conditions from clamped-clamped ends to clamped-free ends (mechanical boundary conditions) cause changes at about 10 percent in the control-ability of FG cylinder.

$$\zeta = \frac{\left|\left|\varphi(0,L/2)\right| - \left|\varphi^{1.25}(0,L/2)\right|\right|}{\left|\varphi^{1.25}(0,L/2)\right|} \times 100 \qquad (34)$$

Figure 13 shows the stress distribution inside the FGPM cylinder along the thickness in the middle of the cylinder length. Shear stress is negligible compared to other stresses in distant areas from boundaries and can be neglected.

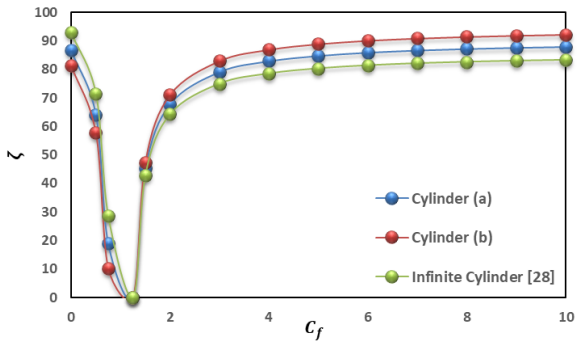

Fig. 12. Result of control gain on the electric potential behavior of FG cylinders in z=0 (n = -2).

Circumferential stress has a dominant effect among the stresses and has great effect on determining the effective stress behavior calculated based on the von Mises failure theory [21]. Also, the axial stress caused by the existence of the free cylinder head in the cylinder (b) has tension state and compression state distribution.

$$\sigma_{eff} = \frac{1}{\sqrt{2}}\left((\sigma_x - \sigma_\theta)^2 + (\sigma_x - \sigma_z)^2 + (\sigma_z - \sigma_\theta)^2 + 6\tau_{zx}{}^2\right)^{0.5} \qquad (35)$$

Figure 14 shows the effective stress distribution. The maximum amount of effective stress occurs near the boundary areas, which increases with any increase in the heterogeneity constant. As can be seen, the intensity of the heterogeneity constant effect on the cylinder of

type (a) or of the cylinder with two constrained heads is greater and causes more changes.

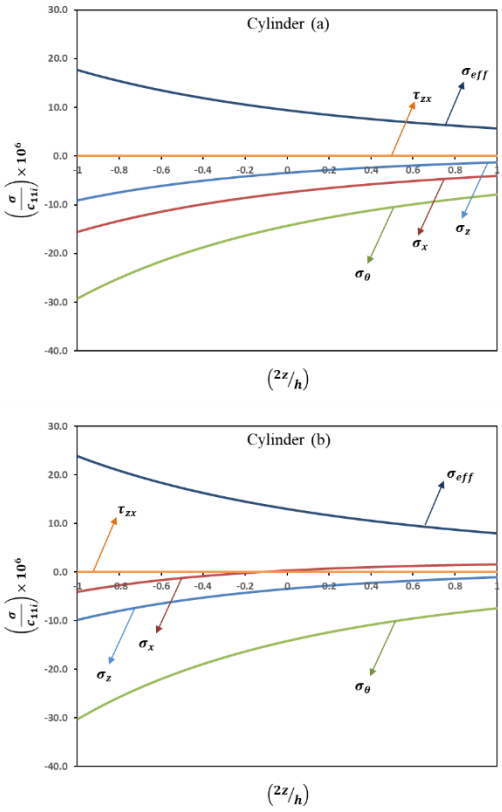

Fig. 13. Distribution of stresses in the middle of FGPM cylinders length (C_f=0, n=-2).

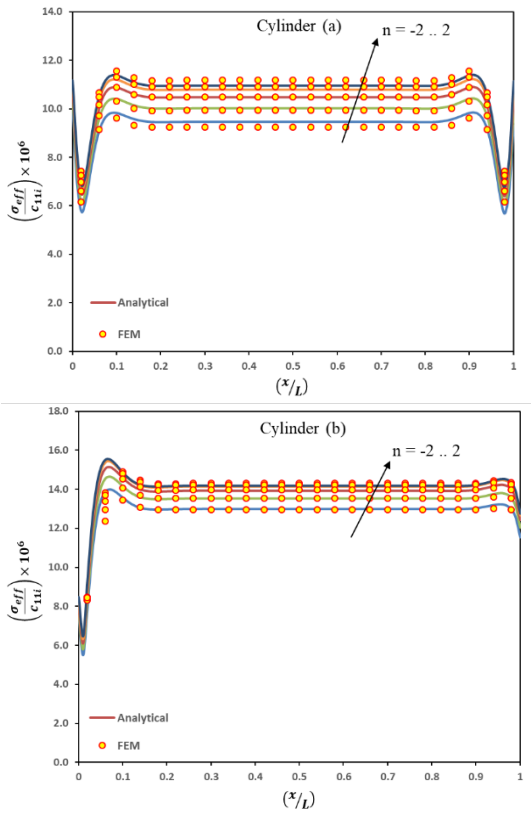

Fig. 14. Distribution of effective stress in the middle layers of FGPM cylinders (C_f=0).

Figure 15 shows the effect of control gain on the effective stress in the middle layer of heterogeneous cylinders. Generally, the effect of control gain on the effective stress is negligible except in the upper cylinder head that the voltage is applied on it. Special attention should be considered for the head of cylinder with applied voltage when it was designed.

Figure 16 shows the distribution of the electric field along the axial direction in heterogeneous cylinders. The heterogeneity constant has no observable effect on the distribution of the electric field along the axial direction. As it is seen, the largest distribution of the electric field occurs in the vicinity of the boundaries or within the boundaries themselves, requiring more attention to these areas.

$$E = \sqrt{E_x^{\ 2} + E_z^{\ 2}} \tag{36}$$

Figure 17 shows the of control gain on electric field in the middle layers of heterogeneous cylinders, which is calculated according to the Eq. (35). As it is seen, the effect of control gain on electric field.is remarkable at the upper head or applied voltage head. Therefore, the designers should pay special attention to this head.

Table 2 shows the results of solving analytical and finite element problems using the ANSYS 12.0 software. As can be seen, there is a good consensus between the predicted results of the two methods that showed in Figs. 6, 7, 10 and 14.

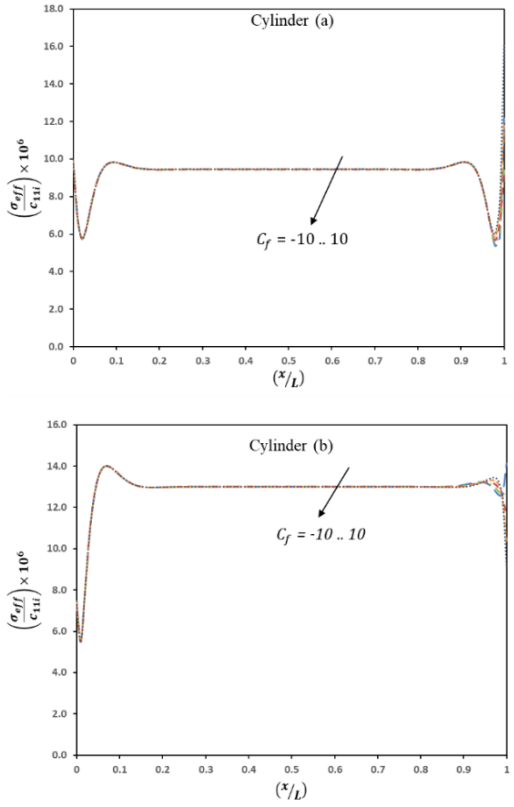

Fig. 15. Result of control gain on effective stress in the middle layer of FG cylinders (n = -2).

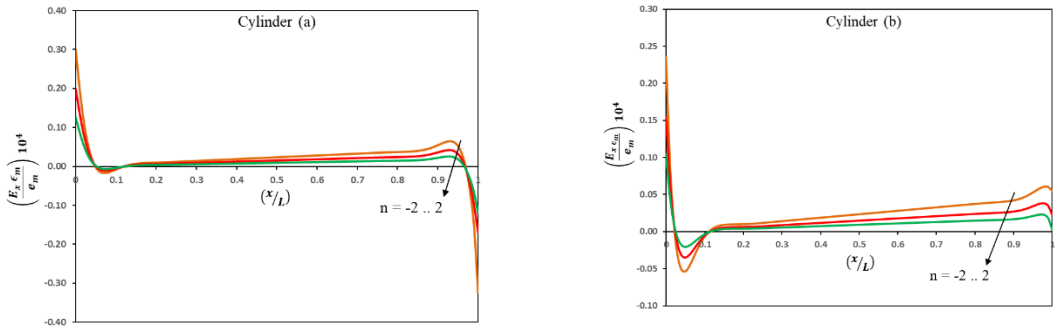

Fig. 16. Distribution of axial component of electric field in the middle layers of FGPM cylinders (C_f =0).

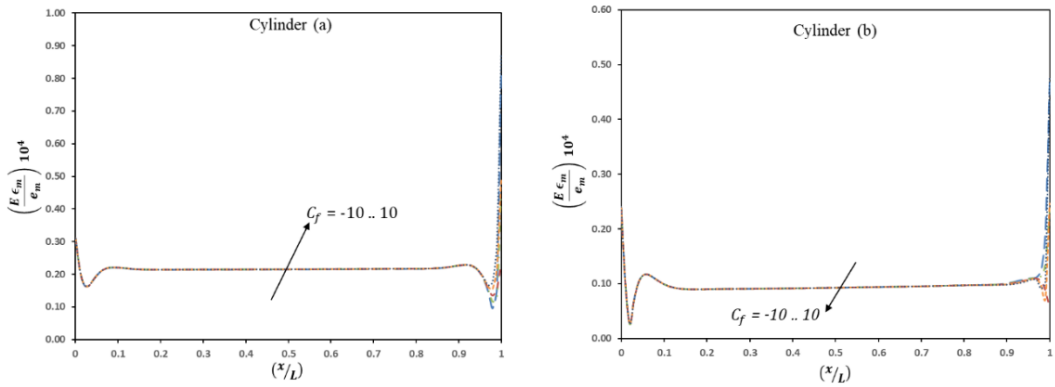

Fig. 17. Result of control gain on electric field in the middle layers of FG cylinders (n = -2).

Table 2. The numerical results achieved for analytical solution and FE solution of FGPM cylinders (x=L/2, C_f =0).

			Cylinder (a)			Cylinder (b)		
			n = -2	n = 0	n = 2	n = -2	n= 0	n = 2
Inner Layer	U_r (mm)	Analytical	-0.001007	-0.000706	-0.000469	-0.001344	-0.000931	-0.000612
		FEM	-0.001039	-0.000726	-0.000481	-0.001379	-0.000954	-0.000626
		Difference (%)	3.07	2.75	2.49	2.54	2.41	2.24
Outer layer	U_r (mm)	Analytical	-0.000942	-0.000654	-0.000430	-0.001340	-0.000919	-0.000598
		FEM	-0.000977	-0.000667	-0.000435	-0.001379	-0.000935	-0.000604
		Difference (%)	3.58	1.95	1.15	2.83	1.71	0.99
Inner layer	σ_{eff} (MPa)	Analytical	2.0423	1.4482	0.9705	2.7429	1.8936	1.2406
		FEM	2.6202	1.8776	1.2748	3.0646	2.1750	1.4647
		Difference (%)	22.06	22.87	23.87	10.50	12.94	15.30
Outer layer	σ_{eff} (MPa)	Analytical	0.6552	1.0450	1.5751	0.9194	1.4110	2.0583
		FEM	0.4857	0.8540	1.3526	0.9325	1.3792	1.9697
		Difference (%)	34.89	23.37	16.45	1.40	2.31	4.50
Inner layer	φ (V)	Analytical	1102.63	660.44	373.45	1703.42	1079.73	644.34
		FEM	1114.90	660.74	368.53	1576.90	993.18	587.14
		Difference (%)	1.10	0.05	1.33	8.02	8.71	9.74
Outer layer	φ (V)	Analytical	1636.92	1043.48	632.10	1927.67	1258.94	775.98
		FEM	1639.20	1068.10	656.11	1833.60	1227.40	768.52
		Difference (%)	0.14	2.30	3.66	5.13	2.57	0.97

5. Conclusions

In this study, Active control and the two-dimensional analytical solution of piezoelectric FGM cylinders under mechanical and electrical loading in their internal and external layers and different boundary conditions in two cylinder's heads Using First-Order Electric Potential Theory and a voltage feedback control method was presented. A numerical study was carried out for the two states of boundary conditions: (a) two clamped heads; and (b) one lower clamped head and the upper free head, and the effects of heterogeneity, control gain, boundary conditions, and electromechanical loading were studied. Then, the results of this study were compared with the results obtained from FEM, which showed a good agreement between the findings. The results of this study can be summarized as follows.

1. The present study presents a two-dimensional analytical solution for the electrical and mechanical field, which, unlike other previous studies of two-dimensional analyzes, is not a series solution method of differential equations, and there is no need to investigate the convergence of the response. Therefore, it is of less computational volume and higher accuracy and takes less time for computation. Furthermore, it is not specific to the special mechanical boundary conditions in the two cylinder's heads and is able to answer different boundary conditions in the two cylinder's heads. It is clear that the above method can easily be used to achieve the optimal values of heterogeneity constant, control gain and type of support conditions in the structure.

2. Reviewing and comparing the results of two analytical and finite element methods shows that using the first-order theory of electric potential reliable and useful and predicts the results accurately. However, when the computing time and volume increase are considered to be of lower priority than higher accuracy in calculations, one can use higher-order theory of electric field potential and displacement field.

3. The results show that unlike the displacement field that has no significant changes in areas far from the boundary in the direction of cylinder thickness, the displacement field behavior can be assumed to be independent of thickness, however, electric potential changes even in the areas far from the boundaries cause significant changes in line with the thickness. Therefore, a two-dimensional mechanical-electrical analysis of short-cylindrical piezoelectric cylindrical sensors, actuators and controllers with boundary conditions in both heads is of special importance.

4. The results show that the heterogeneity constant has significant effects on displacements, electric potential, and effective stress (based on von Mises failure theory). By increasing the heterogeneity constant, the displacement field and electric potential value in the cylinder are reduced, but the effective stress increases in the cylinder. Therefore, in the design of such structures, it is necessary to look for an optimal heterogeneity constant because, with a steady reduction of heterogeneity constant besides creating a lower displacement in the structure, more stress is also created, which is an undesirable factor in the design.

5. Investigating and evaluating the results of the cylinders with different boundary conditions in both heads showed that the maximum absolute value of the mechanical and electrical behavior parameters of the cylinders (displacement field, electric potential, stresses and electric field) occurs near the boundaries or at the cylinder boundaries. Therefore, designers and engineers should pay special attention to the border areas and nearby locations.

6. The results show that the control gain has remarkable influence on the electric potential behavior. However, the other parameters are significantly affected only in cylinders head where the voltage is applies. However, it may ignore the effect of control gain on displacements, stress and electrical field in the faraway region of FG cylinder from the heads, but designers or engineers should be careful when applied voltage for control electric potential in structure because it significantly affects the mechanical and electrical behavior in heads where the voltage is applied.

7. Considering FG cylinders with different mechanical boundary conditions shows that it affects the controllability of FG cylinders, and based on the value of control gain, it can increase or decrease the controllability. In the short length cylinder, this issue should be considered in design and calculations.

Appendix

Non-zero components of $\tilde{A}_{6\times6}$ matrix are calculated as follows:

$$\begin{cases} \tilde{A}_{2\times4}=-\int_{-\frac{h}{2}}^{\frac{h}{2}} c_{22i}\frac{(R+z)^{n+1}}{(R-h/2)^n}z^2\,dz;\ \tilde{A}_{3\times1}=-\int_{-\frac{h}{2}}^{\frac{h}{2}} K_s c_{55i}\frac{(R+z)^{n+1}}{(R-h/2)^n}dz;\ \tilde{A}_{3\times2}=\tilde{A}_{4\times1}=-\int_{-\frac{h}{2}}^{\frac{h}{2}} K_s c_{55i}\frac{(R+z)^{n+1}}{(R-h/2)^n}z\,dz; \\ \tilde{A}_{3\times6}=-\int_{-\frac{h}{2}}^{\frac{h}{2}} K_s e_{35i}\frac{(R+z)^{n+1}}{(R-h/2)^n}z\,dz;\ \tilde{A}_{4\times2}=-\int_{-\frac{h}{2}}^{\frac{h}{2}} K_s c_{55i}\frac{(R+z)^{n+1}}{(R-h/2)^n}z^2\,dz;\ \tilde{A}_{4\times6}=-\int_{-\frac{h}{2}}^{\frac{h}{2}} K_s e_{35i}\frac{(R+z)^{n+1}}{(R-h/2)^n}z^2\,dz; \\ \tilde{A}_{6\times1}=-\int_{-\frac{h}{2}}^{\frac{h}{2}} e_{35i}\frac{(R+z)^{n+1}}{(R-h/2)^n}z\,dz;\ \tilde{A}_{6\times2}=-\int_{-\frac{h}{2}}^{\frac{h}{2}} e_{35i}\frac{(R+z)^{n+1}}{(R-h/2)^n}z^2\,dz;\ \tilde{A}_{6\times6}=\int_{-\frac{h}{2}}^{\frac{h}{2}} \in_{22i}\frac{(R+z)^{n+1}}{(R-h/2)^n}z^2\,dz; \end{cases} \tag{A1}$$

Which in the above relations K_s is the shear correction coefficient and is equal to 5/6 [7]. Also, for the non-zero components of $\tilde{B}_{6\times6}$ matrix we have:

$$\begin{cases} \tilde{B}_{1\times4}=-\tilde{B}_{2\times3}=\int_{-\frac{h}{2}}^{\frac{h}{2}} c_{22i}\frac{(R+z)^{n+1}}{(R-h/2)^n}z\,dz;\ \tilde{B}_{2\times1}=-\tilde{B}_{3\times4}=\int_{-\frac{h}{2}}^{\frac{h}{2}}\left(K_s c_{55i}(R+z)-z c_{23i}\right)\frac{(R+z)^n}{(R-h/2)^n}z\,dz; \\ \tilde{B}_{2\times2}=-\tilde{B}_{4\times4}=\int_{-\frac{h}{2}}^{\frac{h}{2}}\left(K_s c_{55i}-c_{12i}-\frac{z c_{23i}}{(R+z)}\right)\frac{(R+z)^{n+1}}{(R-h/2)^n}z\,dz;\ \tilde{B}_{2\times6}=\int_{-\frac{h}{2}}^{\frac{h}{2}}\left(K_s z e_{35i}-z e_{12i}\right)\frac{(R+z)^{n+1}}{(R-h/2)^n}dz; \\ \tilde{B}_{3\times5}=-\int_{-\frac{h}{2}}^{\frac{h}{2}} K_s\, e_{35i}\frac{(R+z)^{n+1}}{(R-h/2)^n}dz;\ \tilde{B}_{4\times5}=-\int_{-\frac{h}{2}}^{\frac{h}{2}} K_s\, e_{35i}\frac{(R+z)^{n+1}}{(R-h/2)^n}z\,dz;\ \tilde{B}_{5\times1}=\int_{-\frac{h}{2}}^{\frac{h}{2}} e_{35i}\frac{(R+z)^{n+1}}{(R-h/2)^n}dz; \\ \tilde{B}_{5\times2}=\int_{-\frac{h}{2}}^{\frac{h}{2}} e_{35i}\frac{(R+z)^{n+1}}{(R-h/2)^n}z\,dz;\ \tilde{B}_{5\times6}=-\tilde{B}_{6\times5}=-\int_{-\frac{h}{2}}^{\frac{h}{2}} \in_{22i}\frac{(R+z)^{n+1}}{(R-h/2)^n}z\,dz;\ \tilde{B}_{6\times4}=\int_{-\frac{h}{2}}^{\frac{h}{2}}\left(e_{12i}-e_{35i}\right)z\frac{(R+z)^{n+1}}{(R-h/2)^n}dz; \end{cases} \tag{A2}$$

And for $\tilde{C}_{6\times6}$ matrix non-zero components, we have:

$$\begin{cases} \tilde{C}_{1\times1}=\tilde{C}_{3\times3}=\int_{-\frac{h}{2}}^{\frac{h}{2}} c_{23i}\frac{(R+z)^n}{(R-h/2)^n}dz;\ \tilde{C}_{1\times2}=\tilde{C}_{4\times3}=\int_{-\frac{h}{2}}^{\frac{h}{2}}\left(c_{12i}+\frac{z c_{23i}}{(R+z)}\right)\frac{(R+z)^{n+1}}{(R-h/2)^n}dz;\ \tilde{C}_{1\times3}=\int_{-\frac{h}{2}}^{\frac{h}{2}} c_{22i}\frac{(R+z)^{n+1}}{(R-h/2)^n}dz; \\ \tilde{C}_{1\times6}=\int_{-\frac{h}{2}}^{\frac{h}{2}} e_{12i}\frac{(R+z)^{n+1}}{(R-h/2)^n}dz;\ \tilde{C}_{2\times4}=\int_{-\frac{h}{2}}^{\frac{h}{2}} K_s c_{55i}\frac{(R+z)^{n+1}}{(R-h/2)^n}dz;\ \tilde{C}_{2\times5}=\int_{-\frac{h}{2}}^{\frac{h}{2}} K_s e_{35i}\frac{(R+z)^{n+1}}{(R-h/2)^n}dz;\ \tilde{C}_{3\times1}=\int_{-\frac{h}{2}}^{\frac{h}{2}} c_{22i}\frac{(R+z)^{n-1}}{(R-h/2)^n}dz; \\ \tilde{C}_{3\times2}=\tilde{C}_{4\times1}=\int_{-\frac{h}{2}}^{\frac{h}{2}}\left(c_{12i}+\frac{z c_{22i}}{(R+z)}\right)\frac{(R+z)^n}{(R-h/2)^n}dz;\ \tilde{C}_{3\times6}=\tilde{C}_{6\times1}=\int_{-\frac{h}{2}}^{\frac{h}{2}} e_{12i}\frac{(R+z)^n}{(R-h/2)^n}dz;\ \tilde{C}_{4\times2}=\int_{-\frac{h}{2}}^{\frac{h}{2}}\left(2c_{12i}+\frac{c_{11i}}{z}(R+z)+\frac{z c_{22i}}{(R+z)}\right)z\frac{(R+z)^n}{(R-h/2)^n}dz; \\ \tilde{C}_{4\times6}=\tilde{C}_{6\times2}=\int_{-\frac{h}{2}}^{\frac{h}{2}}\left(e_{11i}+\frac{z e_{12i}}{(R+z)}\right)\frac{(R+z)^{n+1}}{(R-h/2)^n}dz;\ \tilde{C}_{5\times4}=\int_{-\frac{h}{2}}^{\frac{h}{2}} e_{35i}\frac{(R+z)^{n+1}}{(R-h/2)^n}dz; \\ \tilde{C}_{5\times5}=-\int_{-\frac{h}{2}}^{\frac{h}{2}} \in_{22i}\frac{(R+z)^{n+1}}{(R-h/2)^n}dz;\ \tilde{C}_{6\times3}=\int_{-\frac{h}{2}}^{\frac{h}{2}} e_{12i}\frac{(R+z)^{n+1}}{(R-h/2)^n}dz;\ \tilde{C}_{6\times6}=-\int_{-\frac{h}{2}}^{\frac{h}{2}} \in_{11i}\frac{(R+z)^{n+1}}{(R-h/2)^n}dz; \end{cases} \tag{A3}$$

Quasi-vector non-zero components $\vec{F}_{6\times1}$ are calculated as follows:

$$\begin{cases} F_3=P_i\left(R-\frac{h}{2}\right)-P_o\left(R+\frac{h}{2}\right) \\ F_4=\frac{h}{2}\left(P_i\left(\frac{h}{2}-R\right)-P_o\left(R+\frac{h}{2}\right)\right) \\ F_5=Q_i\left(R-\frac{h}{2}\right)+Q_o\left(R+\frac{h}{2}\right) \\ F_6=\frac{h}{2}\left(Q_i\left(R-\frac{h}{2}\right)-Q_o\left(R+\frac{h}{2}\right)\right) \end{cases} \tag{A4}$$

References

[1] Ventsel E. and Krauthammer T., 2001. *Thin Plates and Shells: Theory, Analysis, and Applications*, Marcel Dekker Company.

[2] Tzou H.S., Lee H.-J. and Arnold S., 2004. Smart materials, precision sensors/actuators, smart structures, and structronic systems, *Mechanics of Advanced Materials and Structures*, *11*, pp. 367-393.

[3] Dai H.L, Hong L., Fu Y.M. and Xiao X., 2010. Analytical Solution for Electromagnetothermoelastic Behaviors of a Functionally Graded Piezoelectric Hollow Cylinder, *Applied Mathematical Modelling 34*, pp. 343–357.

[4] Ghannad M. and Zamani-Nejad M., 2010. Elastic Analysis of Pressurized Thick Hollow Cylindrical Shells with Clamped-Clamped Ends, *Mechanika, 85*, pp. 11-18.

[5] Ghorbanpour Arani A., Jafarzadeh Jazi A., Abdollahian M., Mozdianfard M.R., Mohammadimehr M. and Amir S., 2011. Exact Solution for Electrothermoelastic Behaviors of a Radially Polarized FGPM Rotating Disk, *Journal of Solid Mechanics, 3*, pp. 244-257.

[6] Ghannad M. and Zamani-Nejad M., 2012. Complete Elastic Solution of Pressurized Thick Cylindrical Shells Made of Heterogeneous Functionally Graded Materials, *Mechanika, 18*, pp. 640-649.

[7] Ghannad M. and Zamani-Nejad M., 2012. Elastic Analysis of Heterogeneous Thick Cylinders Subjected to Internal or External Pressure Using Shear Deformation Theory, *Acta Polytechnica Hungarica, 9*, pp. 117-136.

[8] Dai H.-L. and Jiang H.-J., 2013. Analytical study for electromagnetothermoelastic behavior of a functionally graded piezoelectric solid cylinder, *Mechanics of Advanced Materials and Structures, 20*, pp. 811-818.

[9] Kargarnovin M.H., Hashemi R. and Emami A.A., 2013. Electroelastic Analysis of FG Piezoelectric Structures under Thermo-Electro-Mechanical Loadings, *Mechanics of Advanced Materials and Structures, 20*, pp. 11-27.

[10] Ghannad M. and Gharooni H., 2014. Displacements and Stresses in Pressurized Thick FGM Cylinders with Exponentially Varying Properties Based on FSDT, *Structural Engineering and Mechanics, 51*, pp. 939-953.

[11] Ghannad M. and Gharooni H., 2015. Thermo-Elastic Analysis of Clamped-Clamped Thick FGM Cylinders by Using Third-Order Shear Deformation Theory, *Latin American Journal of Solids and Structures, 12*, pp. 1024-1041.

[12] Khorshidi K. and Bakhsheshy A., 2014. Free natural frequency analysis of an FG composite rectangular plate coupled with fluid using Rayleigh–Ritz method, *Mechanics of Advanced Composite Structures*, *1*(2), pp. 131-143.

[13] Saviz M.R., 2015. Elasticity Solution of a Laminated Clamped Cylindrical Shell with Piezoelectric Layer under Dynamic Load, *Mechanics of Advanced Materials and Structures, 22*, pp. 503-519.

[14] Jabbari M. and Aghdam M. B., 2015. Asymmetric Thermal Stresses of Hollow FGM Cylinders with Piezoelectric Internal and External Layers, *Journal of Solid Mechanics, 7*, pp. 327–343.

[15] Khorshidi K., Asgari T. and Fallah A., 2015. Free vibrations analysis of functionally graded rectangular nano-plates based on nonlocal exponential shear deformation theory, *Mechanics of Advanced Composite Structures*, *2*(2), pp. 79-93.

[16] Atrian A., JafariFesharaki J. and Nourbakhsh S.H., 2015. Thermo-Electromechanical Behavior of Functionally Graded Piezoelectric Hollow Cylinder under Non-Axisymmetric Load, *Applied Mathematics and Mechanics (English Edition), 36*, pp. 939-954.

[17] Khorshidi K., Rezaei E., Ghadimi A. A. and Pagoli M., 2015. Active vibration control of circular plates coupled with piezoelectric layers excited by plane sound wave, *Applied Mathematical Modelling, 39*(3-4), pp. 1217-1228.

[18] Khorshidi K., Balali M. and Ghadimi A. A., 2015. Control Forced Vibrations Of Laminated Composite Rectangular Plate Resting On Linear Line Support, *Modares Mechanical Engineering, 15*(9), pp. 95-104.

[19] Loghman A. and Parsa H., 2016. Closed Form Solution for Electro-Magneto-Thermo-Elastic Behaviour of Double-Layered Composite Cylinder, *Journal of Solid Mechanics, 8*, pp. 31-44.

[20] Ghannad M. and Parhizkar Yaghoobi M., 2015. A Thermoelasticity Solution for Thick Cylinders Subjected to Thermo-Mechanical Loads Under Various Boundary Conditions, *International Journal of Advanced Design and Manufacturing Technology, 8*, pp. 1-12.

[21] Ghannad M. and Parhizkar Yaghoobi M., 2017. 2D Thermo Elastic Behavior of a FG Cylinder under Thermomechanical Loads Using a First Order Temperature Theory, *International Journal of Pressure Vessels and Piping, 149*, pp. 75-92.

[22] Arefi M., Karroubi R. and Irani-Rahaghiand M., 2016. Free vibration analysis of functionally graded laminated sandwich cylindrical shells integrated with piezoelectric layer, *Applied Mathematics and Mechanics (English Edition), 37*(7), pp. 821-834.

[23] Arefi M. and Zenkour A. M., 2017. Size-dependent free vibration and dynamic analyses of piezo-electromagnetic sandwich nanoplates resting on viscoelastic foundation, *Physica B, 521*, pp. 188-197.

[24] Khorshidi K. and Pagoli M., 2016. Analytical solution for sound radiation of vibrating circular plates coupled with piezo-electric layers, *Mechanics of Advanced Composite Structures*, *3*(2), pp. 89-98.

[25] Alibeigloo A., 2018. Thermo Elasticity Solution of Functionally Graded, Solid, Circular, and Annular Plates Integrated with Piezoelectric Layers Using the Differential Quadrature Method, *Mechanics of Advanced Materials and Structures, 25*, pp. 766-84.

[26] Mehditabar A., Rahimi G.H. and Tarahhomi M.H., 2018. Thermo-Elastic Analysis of a Functionally Graded Piezoelectric Rotating Hollow Cylindrical Shell Subjected to Dynamic Loads, *Mechanics of Advanced Materials and Structures, 25*, pp. 1068-1079.

[27] Khorshidi K., Siahpush A. and Fallah A., 2017. Electro-mechanical free vibrations analysis of composite rectangular piezoelectric nanoplate using modified shear deformation theories, *Journal of Science and Technology of Composites, 4*(2), pp. 151-160.

[28] Parhizkar Yaghoobi M., Ghaffari I. and Ghannad M., 2018. Stress and active control analysis of functionally graded piezoelectric material cylinder and disk under electro-thermo-mechanical loading, *Journal of Intelligent Material Systems and Structures, 29*(5), pp. 924-937.

[29] Arefi M. and Mohammad-Rezaei Bidgoli E., 2018. Electro-elastic displacement and stress analysis of the piezoelectric doubly curved shells resting on Winkler's foundation subjected to applied voltage, *Mechanics of Advanced Materials and Structures, 0*(0), pp. 1-14.

[30] Ghasemi A. R. and Hosseinpour K., 2018. Creep Strain and Stress Analysis in Laminated Composite Pressure Vessels, *Mechanics of Advanced Composite Structures*, *5*(2), pp. 141-147.

[31] Arefi M., Mohammadi M., Amir-Ahmadi S. and Rabczuk T., 2019. FSDT electro-elastic analysis of FG-CNTRC cylindrical three-layered pressure vessels with piezoelectric face-sheets, *Thin-Walled Structures, 144*, p. 106320.

[32] Arefi M., Mohammadi M. and Rabczuk T., 2019. Effect of Characteristics and Distribution of Porosity on Electro-Elastic Analysis of Laminated Vessels with Piezoelectric Face-Sheets Based on Higher Order Modeling, *Composite Structures, 225*, p. 111085.

[33] Mohammadi M., Arefi M and Amir-Ahmadi S., 2020. Two-Dimensional Electro-Elastic Analysis of FG-CNTRC Cylindrical Laminated Pressure Vessels with Piezoelectric Layers Based on Third-Order Shear Deformation Theory, *Journal of Pressure Vessel Technology, 142*(2), p. 021304.

[34] Ghasemi A. R. and Hosseinpour K., 2018. Thermo-Magneto-Mechanical Long-Term Creep Behavior of Three-Phase Nano-Composite Cylinder, *Composites Science and Technology, 167*, pp. 71-78.

[35] Hosseinpour K. and Ghasemi A. R., 2019. Effects of Magnetic Field in Creep Behavior of Three-Phase Laminated Composite Cylindrical Shells, *Mechanics of Advanced Composite Structures 6*(1), pp. 51-56.

[36] Khorshidi K., and Karimi M., 2020. Fluid-Structure Interaction of Vibrating Composite Piezoelectric Plates Using Exponential Shear Deformation Theory, *Mechanics of Advanced Composite Structures*, *7*(1), pp. 59-69

[37] Benjeddou A., 2000. Advances in Piezoelectric Finite Element Modeling of Adaptive Structural Elements: a Survey, *Computers and Structures, 76*, pp. 347-363.

[38] Wang X. and Zhong Z., 2003. The General Solution of Spherically Isotropic Magnetoelectroelastic Media and Its Applications, *European Journal of Mechanics A/Solids, 22*, pp. 953-969.

[39] Benjeddou A. and Andrianarison O., 2005. A Thermopiezoelectric Mixed Variational Theorem for Smart Multilayered Composites, *Computers and Structures, 83*, pp. 1266-1276.

[40] Ghaffari I., Parhizkar Yaghoobi M. and Ghannad M., 2018. Complete Mechanical Behavior Analysis of FG Nano Beam under Non-Uniform Loading Using Non-Local Theory, *Materials Research Express, 5*(1), p. 015016.

[41] Li J. and Li F., 2019. Active Control of Thermal Buckling for Plates Using a Temperature Feedback Control Method, *Smart Materials and Structures, 28*(4), p. 045001.

[42] Yang J., 2006. The Mechanics of Piezoelectric Structures, World Scientific.

[43] Ye Z.G., 2008. Handbook of Dielectric, Piezoelectric and Ferroelectric Materials: Synthesis, Properties and Applications, CRC Press.